Bubbly Two-Phase Flow in Hydraulic Jumps at Large Froude Numbers

Hubert Chanson[1]

Abstract: A hydraulic jump is a sudden, rapid transition from a supercritical flow to a subcritical flow. At large inflow Froude numbers, the jump is characterized by a significant amount of entrained air. For this paper, the bubbly two-phase flow properties of steady and strong hydraulic jumps were investigated experimentally. The results demonstrate that the strong air entrainment rate and the depth-averaged void-fraction data highlight a rapid deaeration of the jump roller. The results suggest that the hydraulic jumps are effective aerators and that the rate of detrainment is comparatively smaller at the largest Froude numbers. **DOI: 10.1061/(ASCE)HY.1943-7900.0000323.** © *2011 American Society of Civil Engineers.*

CE Database subject headings: Hydraulic jump; Two phase flow; Froude number; Hydraulic models.

Author keywords: Hydraulic jumps; Bubbly two-phase flow; Froude numbers; Physical modeling.

Introduction

The hydraulic jump is a classical flow situation defined as the rapid transition from a supercritical open-channel flow to a subcritical flow. At prototype scales, the jump is characterized by a highly turbulent flow region with macroscale vortices, which is called the roller, associated with significant kinetic energy dissipation and a bubbly two-phase flow region. Fig. 1 shows hydraulic jumps for different inflow conditions, highlighting the substantial aeration of the roller. The bubbly two-phase flow is caused by the strong interaction between the turbulence structures and the free-surface at the impingement of the supercritical flow with the roller, leading to some air entrapment. Generally, the air bubble entrainment takes place at the point at which the turbulent stresses overcome both surface tension and viscous forces (Ervine and Falvey 1987; Chanson 1997).

Bubbly flow measurements in hydraulic jumps were first performed by Rajaratnam (1962). Resch et al. (1974) and Babb and Aus (1981) conducted some hot-film probe measurements in the bubbly flow region, and Resch et al. (1974) showed the effects of upstream flow conditions of the air-water flow properties in the jump roller. Chanson (1995) highlighted the presence of a local maximum void fraction in the shear layer of hydraulic jumps with partially developed inflow; that is, at the point at which the upstream flow is not fully developed, and the turbulent boundary layer does not extend up to the free surface. Chanson and Brattberg (2000) and Murzyn et al. (2005, 2007) showed some seminal bubbly flow features in steady and in weak hydraulic jumps, respectively. Turbulence measurements in hydraulic jumps were also conducted by Rouse et al. (1959), Liu et al. (2004), Chanson (2007), and Kucukali and Chanson (2008); although the first study was conducted in a wind tunnel, and the second was restricted to low Froude numbers (i.e., $F_1 < 3.3$).

Despite these advances, the knowledge of the bubbly two-phase flow region remains limited. The present study examines in detail the two-phase flow properties in hydraulic jumps. Experimental results conducted in a relatively large facility and covering a wide range of inflow Froude numbers were analyzed. It is the aim of this work to characterize the bubbly flow properties in steady and strong hydraulic jumps.

Dimensional Considerations

An experimental investigation performed with geometrically similar models must be made on the basis of a sound similitude. For a hydraulic jump in a horizontal rectangular channel, a dimensional analysis shows that the parameters affecting the air-water flow properties at a position (x, y) include the fluid properties, the channel properties, and the inflow condition properties (Wood 1991; Chanson 1997). After limited simplifications, it yields a series of dimensionless relationships for the two-phase flow properties (Chanson and Gualtieri 2008)

$$C, \frac{F \times d_1}{V_1}, \frac{V}{V_1}, \ldots = F\left(\frac{x - x_1}{d_1}, \frac{y}{d_1}, \frac{x_1}{d_1}, \frac{V_1}{\sqrt{g \times d_1}}, \frac{\rho \times V_1 \times d_1}{\mu}, \frac{g \times \mu^4}{\rho \times \sigma^3}, \frac{W}{d_1}, \frac{\delta}{d_1}, \ldots\right) \quad (1)$$

where C = void fraction; F = bubble count rate; V = velocity; x = coordinate in the flow direction measured from the nozzle; y = vertical coordinate; d_1 and V_1 = upstream flow depth and velocity, respectively; x_1 = distance from the upstream gate; ρ, μ, and σ = water density, dynamic viscosity, and surface tension, respectively; W = channel width; and δ = upstream boundary layer thickness (Fig. 2). Eq. (1) expresses the dimensionless two-phase flow properties (i.e., the terms on the left) at a dimensionless position $(x/d_1, y/d_1)$ within the roller as functions of the dimensionless inflow properties and channel geometry. In the terms on the right, the fourth and fifth terms are the inflow Froude and Reynolds numbers, respectively; and the sixth term is the Morton number. The Morton number is a function only of fluid properties and the gravity

[1]Professor in Civil Engineering, Univ. of Queensland, Brisbane QLD 4072, Australia. E-mail: h.chanson@uq.edu.au

Note. This manuscript was submitted on January 15, 2010; approved on August 18, 2010; published online on September 6, 2010. Discussion period open until September 1, 2011; separate discussions must be submitted for individual papers. This paper is part of the ***Journal of Hydraulic Engineering***, Vol. 137, No. 4, April 1, 2011. ©ASCE, ISSN 0733-9429/2011/4-451–460/$25.00.

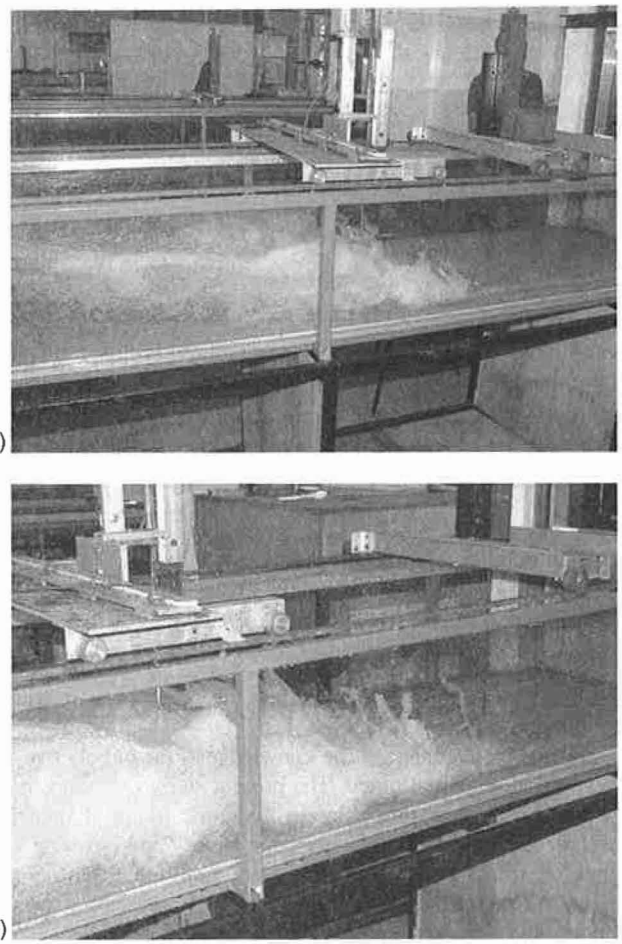

Fig. 1. Air entrainment in hydraulic jumps (photos by Hubert Chanson); (a) $F_1 = 7.5$, $R = 5.6 \times 10^4$, $d_1 = 0.018$ m, $x_1 = 0.75$ m, $x - x_1 = 0.150$ m, and shutter speed = 1/80 s; (b) $F_1 = 10.0$, $R = 7.5 \times 10^4$, $d_1 = 0.018$ m, $x_1 = 0.75$ m, $x - x_1 = 0.350$ m, and shutter speed = 1/80 s

constant. When water and air are used in both the laboratory and the prototype, the Morton number is invariant (Wood 1991; Crowe et al. 1998; Chanson 2009b). The two key dimensionless parameters are the inflow Froude number $F_1 = V_1/\sqrt{g \times d_1}$ and Reynolds number $R = \rho \times q/\mu$, where q = flow rate per unit width.

In an undistorted, geometrically similar model of a hydraulic jump, the dynamic similarity is achieved if each dimensionless parameter has the same value in the model and in the prototype. The turbulent processes and air entrapment in the shear region are dominated by viscous forces. The dynamic similarity of air entrainment in hydraulic jumps becomes impossible because the Froude and Reynolds numbers cannot be equal both in the model and in the prototype unless at full scale. A Froude similitude is commonly used in the study of hydraulic jump, and the Reynolds numbers are typically smaller in laboratory conditions (Henderson 1966). A number of studies showed that the air entrainment in small-size laboratory models might be drastically underestimated (Rao and Kobus 1971; Wood 1991; Chanson 1997). Some recent investigations performed Froude-similar experiments with $5.1 < F_1 < 8.5$ and Reynolds numbers between 2.4×10^4 and 9.8×10^4 (Chanson and Gualtieri 2008; Murzyn and Chanson 2008). The results showed some drastic scale effects in the smaller hydraulic jumps ($R < 4 \times 10^4$) for the distributions of void fraction, bubble count rate, and bubble size, but the issue of scale effects is still not settled.

Table 2. Probability Distribution Functions of Bubble Chords in the Shear Layer for $F_1 = 11.2$, $R = 8.3 \times 10^4$, $d_1 = 0.01783$ m, $x_1 = 0.75$ m (Fig. 9)

$x - x_1$ (m)	y/d_1	V (m/s)	C	F (Hz)	Average chord size (mm)	Number of bubbles
0.225	1.04	3.09	0.217	189.1	3.78	8510
	1.32	2.90	0.351	211.9	5.73	9540
	1.60	2.78	0.382	194.2	5.97	8740
0.400	0.76	2.90	0.101	133.8	2.19	6020
	1.32	2.78	0.198	180.8	3.10	8140
	1.88	2.28	0.207	158.0	3.00	7110

Experimental Facility and Instrumentation

The experiments were performed in a horizontal rectangular flume at the Gordon McKay Hydraulics Laboratory at the University of Queensland. The channel length and width were 3.2 m and 0.50 m,

Table 1. Experimental Flow Conditions

Run	Q (m^3/s)	W (m)	x_1 (m)	V_1 (m/s)	d_1 (m)	F_1	R	Remarks
Series 1								General observations
2	0.0147	0.5	0.75	1.55	0.019	3.58	$2.9E+4$	
3	0.0166	0.5	0.75	1.75	0.019	4.05	$3.3E+4$	
1	0.02225	0.5	0.75	2.34	0.019	5.42	$4.4E+4$	
5	0.0282	0.5	0.75	3.13	0.018	7.46	$5.6E+4$	
4	0.03255	0.5	0.75	3.52	0.0185	8.26	$6.5E+4$	
6	0.0367	0.5	0.75	4.08	0.018	9.70	$7.3E+4$	
7	0.0399	0.5	0.75	4.43	0.018	10.55	$7.9E+4$	
8	0.0470	0.5	0.75	5.22	0.018	12.43	$9.3E+4$	
Series 2								Two-phase flow measurements
090331	0.02025	0.5	0.75	2.19	0.0185	5.14	$4.0E+4$	
090317	0.02825	0.5	0.75	3.14	0.018	7.47	$5.6E+4$	
090720	0.03481	0.5	0.75	3.87	0.018	9.21	$6.9E+4$	
090713	0.03780	0.5	0.75	4.20	0.018	10.0	$7.5E+4$	
090414	0.04175	0.5	0.75	4.68	0.01783	11.2	$8.3E+4$	

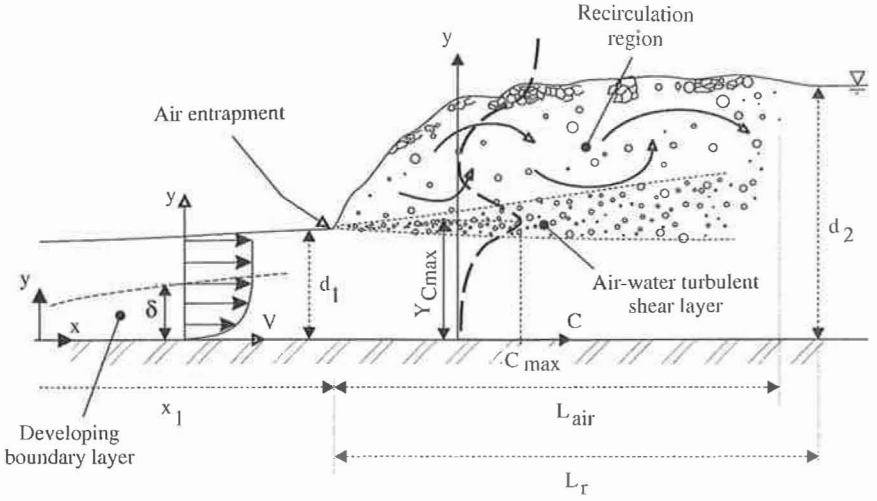

Fig. 2. Definition of the bubbly two-phase flow region in hydraulic jumps

respectively. The sidewall height was 0.45 m. The sidewalls were made of 3.2-m-long glass panels, and the channel bed was made of smooth PVC. This channel was previously used by Chanson (2007), Kucukali and Chanson (2008), and Murzyn and Chanson (2009). Photographs of the experimental facility are shown in Fig. 1, and further details about the apparatus, instrumentation, and data sets are reported in Chanson (2009a).

The water discharge was measured with a Venturi meter installed in the supply line and calibrated in situ with a large V-notch weir. The discharge accuracy was within ±2%. The clear-water flow depths were measured by using rail mounted point gauges within 0.5 mm. The inflow conditions were controlled by a vertical gate with a semicircular shape ($Ø = 0.3$ m). The clear-water velocities were measured with a Prandtl-Pitot tube ($Ø = 3.02$ mm) based on the Prandtl design.

The two-phase flow properties were measured with a double-tip conductivity probe. The conductivity probe is a phase-detection intrusive probe designed to pierce the bubbles. It measures the difference in electrical resistance between air and water (Crowe et al. 1998; Chanson 2002). In the present study, the probe was equipped with two identical sensors with an inner diameter of 0.25 mm. The distance between the probe tips was $\Delta x = 6.96$ mm. The probe was manufactured at the University of Queensland and was previously used in several studies, including Kucukali and Chanson (2008). The displacement and the position of the probe in the vertical direction were controlled by a fine adjustment system connected to a Mitutoyo digimatic scale unit with a vertical accuracy Δy of less than 0.1 mm. A single threshold technique was used for the analysis of the probe signal output; the threshold was set between 45% and 55% of the air-water voltage range. A number of two-phase flow properties were derived from the signal analysis. These included the void fraction C, or air concentration, defined as the volume of air per unit volume of air and water; the bubble count rate F defined as the number of bubbles impacting the probe tip per second; and the bubble chord size distribution. The air-water interfacial velocity V was estimated

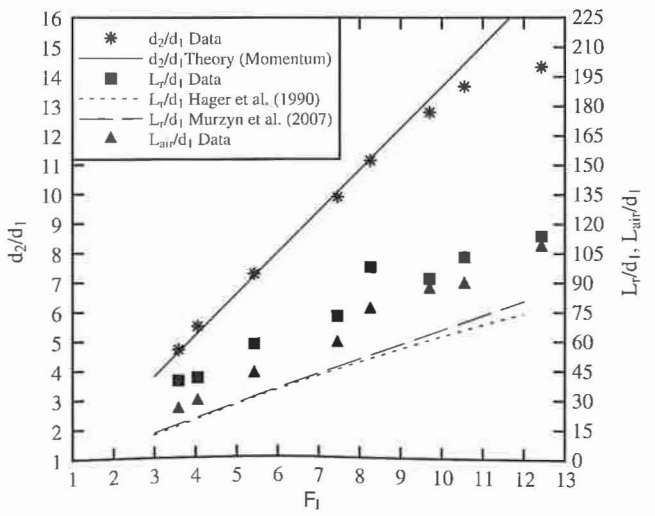

Fig. 3. Ratio of the conjugate depths d_2/d_1, dimensionless roller length L_r/d_1, and bubble flow region length L_{air}/d_1 as functions of the inflow Froude number F_1—Comparison between the experimental data and the solution of the momentum equation

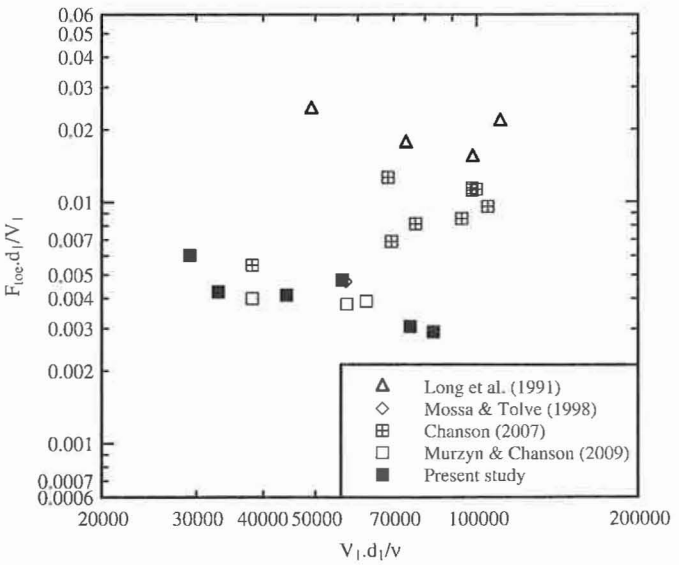

Fig. 4. Jump toe oscillations: Strouhal number data (present study; Long et al. 1991; Mossa and Tolve 1998; Chanson 2007; Murzyn and Chanson 2009)

as $V = \Delta x/T$ where Δx is the longitudinal distance between both tips (i.e, $\Delta x = 6.96$ mm for this study) and T is the average air-water interfacial time between the two probe sensors with T deduced from a cross-correlation analysis (Crowe et al. 1998; Chanson 1997, 2002).

Experimental Flow Conditions

A first series of experiments investigated the general hydraulic jump properties, including upstream and downstream depths and jump toe fluctuation frequency (Table 1). In the second series, some detailed two-phase flow measurements were recorded with the double-tip probe, and the flow conditions are reported in Table 1.

For all experiments, the jump toe was located at $x_1 = 0.75$ m, and the same upstream rounded gate opening $h = 0.018$ m was used for this study. For these conditions, the inflow depth ranged depending upon the flow rate ($d_1 = 0.0178$–0.019 m), as shown in Table 1; and the inflow was characterized by a partially developed boundary layer ($\delta/d_1 = 0.4$–0.6). The upstream flow was little aerated. Some vertical profiles of the void fraction were measured at a location 0.2 m upstream from the jump toe, and the data showed that the depth-averaged void fraction C_{mean} was less than or equal to 0.11, where C_{mean} was defined as

$$C_{mean} = \int_0^{Y_{90}} C \times dy \tag{2}$$

where y = distance normal to the invert; C = local void fraction; and Y_{90} = vertical distance from the bed where $C = 0.9$.

In the present study, the experiments were conducted primarily with large Froude numbers ($F_1 > 7$) and large Reynolds numbers ($R > 5 \times 10^4$).

Basic Flow Patterns

A basic feature of hydraulic jumps is the rapid rise of the free-surface immediately downstream of the jump toe. The free-surface is strongly turbulent with large vertical fluctuations and a bubbly or

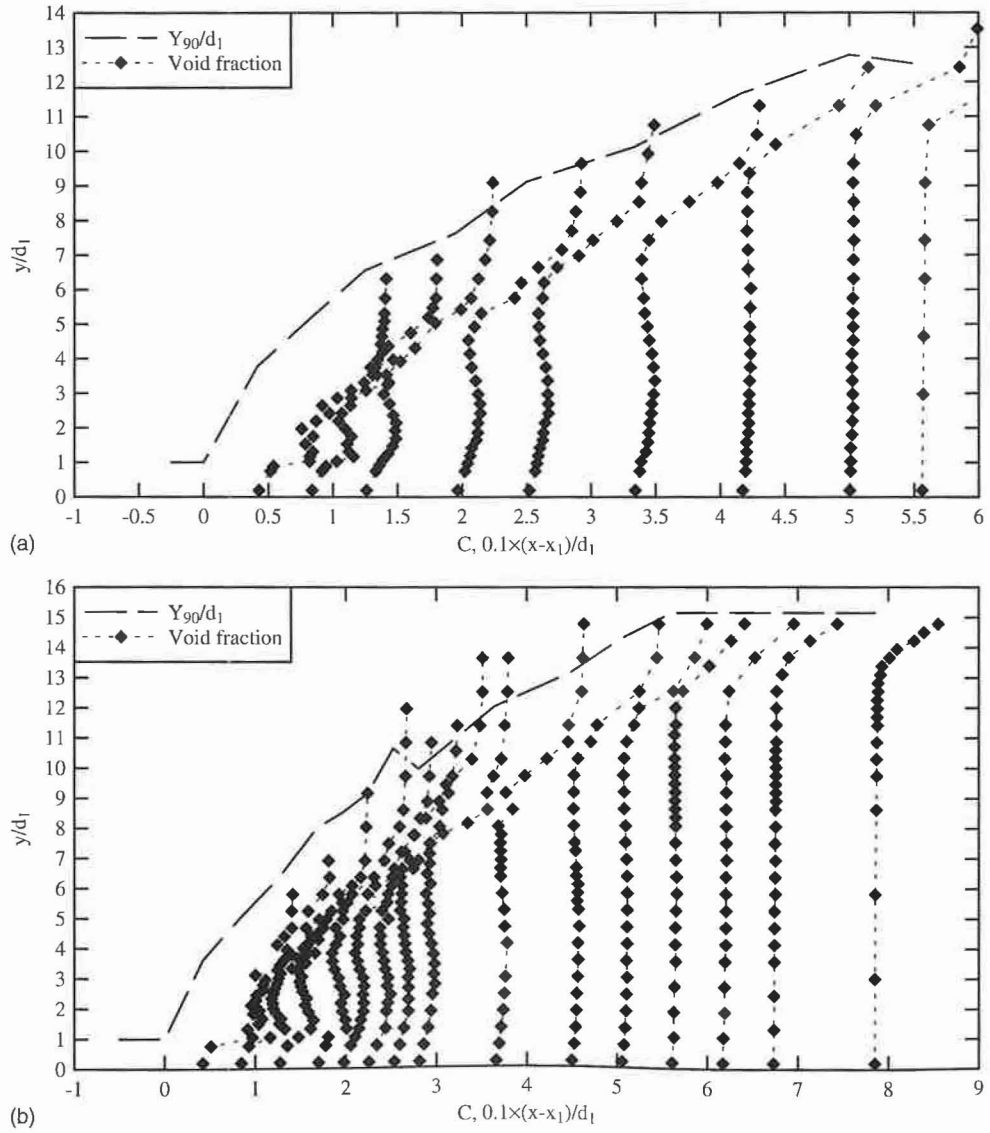

Fig. 5. Dimensionless distribution of void fraction C—Horizontal axis: $0.1 \times (x - x_1)/d_1 + C$; (a) $F_1 = 9.2$, $R = 6.9 \times 10^4$, $d_1 = 0.018$ m, $x_1 = 0.75$ m; (b) $F_1 = 11.2$, $R = 8.3 \times 104$, $d_1 = 0.01783$ m, $x_1 = 0.75$ m

foamy structure, as shown in Fig. 1 for two Froude numbers. Fig. 3 presents the ratio of the downstream to upstream depths d_2/d_1 as a function of the inflow Froude number F_1. The experimental data are compared with the application of the equation of conservation of momentum

$$\frac{d_2}{d_1} = \frac{1}{2} \times (\sqrt{1 + 8 \times F_1^2} - 1) \quad (3)$$

where F_1 = inflow Froude number. Eq. (3) is compared with the experimental observations in Fig. 3, illustrating good agreement except at the largest Froude number. In that case (i.e., $F_1 = 11.2$), the jump roller interfered with the downstream overshot gate.

The dimensionless roller length and bubbly flow region length are also shown in Fig. 3. For this paper, the roller length L_r was defined as the location at which the water surface was quasi-horizontal, and the downstream depth was measured, as shown in Fig. 2. The length L_{air} of the bubbly flow region was determined through some sidewall observations of the entrained air bubbles; that is, L_{air} was the average length of the bubbly flow region. The present data are qualitatively in agreement with the correlations that Hager et al. (1990) and Murzyn et al. (2007) developed for $F_1 < 8$ and 5, respectively; although both correlations tended to underestimate the jump length by 20–30% (Fig. 3). For the present data set, L_r and L_{air} are best correlated by

$$\frac{L_r}{d_1} = 13.7 \times F_1^{0.85} \qquad 5.4 < F_1 < 12.4 \quad (4)$$

$$\frac{L_{air}}{d_1} = 9.54 \times F_1 - 9.1 \qquad 5.4 < F_1 < 12.4 \quad (5)$$

The horizontal oscillations of the jump toe were recorded. These oscillations had relatively small amplitudes, and their frequencies were estimated. The results are presented in Fig. 4 for cases for which the Strouhal number is defined as $S = F_{toe} \times d_1/V_1$ where F_{toe} is the toe oscillation frequency. The data were compared with some earlier studies of jump toe oscillations (Fig. 4). The present jump toe data yielded in average $S \approx 0.005$ that are close to the findings of Mossa and Tolve (1998), Chanson (2007), and Murzyn and Chanson (2009). The comparative results showed that no

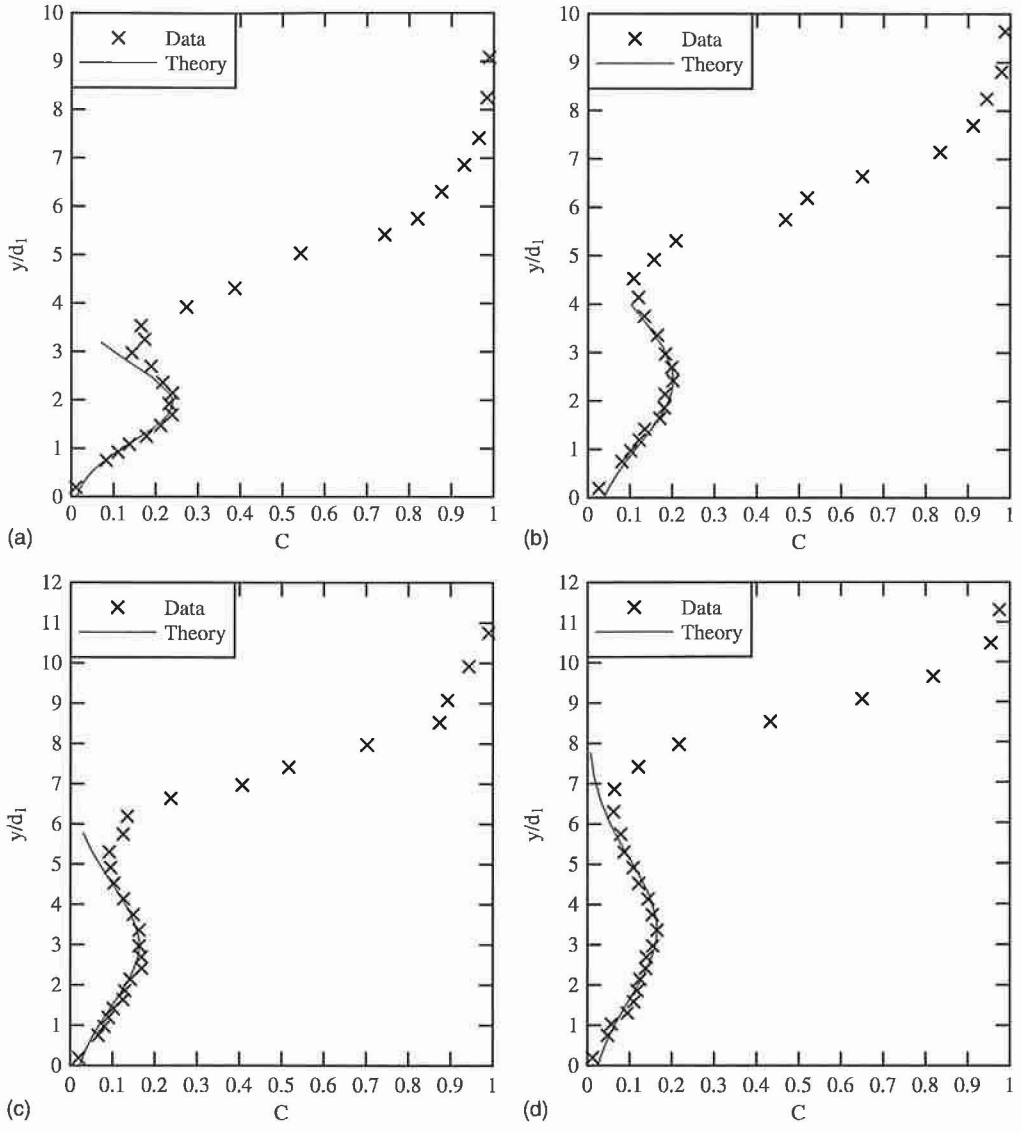

Fig. 6. Void-fraction distributions in a hydraulic jump with partially developed inflow conditions: $x_1 = 0.75$ m, $d_1 = 0.018$ m, $F_1 = 9.2$, $R = 6.9 \times 10^4$, $x - x_1 = 0.225$, 0.30, 0.45, and 0.60 m; comparison between the experimental data (present study) and the mathematical solution; (a) $x - x_1 = 0.225$ m; (b) $x - x_1 = 0.35$ m; (c) $x - x_1 = 0.45$ m; (d) $x - x_1 = 0.60$ m

evident relationship between the Strouhal and the Reynolds numbers exists (Fig. 4).

Bubbly Flow Properties of Hydraulic Jumps

The hydraulic jumps are characterized by strong air bubble entrainment, spray, and splashing (Fig. 1). For this paper, the two-phase flow measurements were conducted for five inflow Froude numbers ranging from 5.1 to 11.2 with a focus on the largest Froude numbers.

In hydraulic jumps with partially developed inflow, the turbulent shear layer corresponds to an advective diffusion region in which the void-fractions distributions exhibit a peak in the turbulent shear region (Resch et al. 1974; Chanson 1995). This is shown in Figs. 5 and 6. Fig. 5 presents some dimensionless distributions of the void fraction along the hydraulic jump for two Froude numbers ($F_1 = 9.2$ and 11.2). The characteristic location Y_{90}/d_1 at which the void fraction equals 0.90 is also shown (i.e., the thick dashed line). It characterized the location of the roller's upper free-surface. Within the roller $y < Y_{90}$, the void-fraction profiles presented a characteristic shape. The void fraction was about zero next to the invert. A local maximum $C = C_{max}$ was observed in the shear layer, as shown in Fig. 2. Close to the free surface, the void fraction increased rapidly toward unity.

In the air-water shear layer, the void-fraction distributions closely followed an analytical solution of the advective diffusion equation for air bubbles (Chanson 1995)

$$C = C_{max} \times \exp\left(-\frac{1}{4 \times D^{\#}} \times \frac{\left(\frac{y - Y_{C\,max}}{d_1}\right)^2}{\left(\frac{x - x_1}{d_1}\right)}\right) \quad (6)$$

where $D^{\#}$ = dimensionless diffusivity $D^{\#} = D_t/(V_1 \times d_1)$; D_t = air bubble diffusivity; d_1 and V_1 = inflow depth and velocity, respectively; and $Y_{C\,max}$ = distance from the bed in which $C = C_{max}$ (Fig. 2). Eq. (6) was compared with data from Fig. 6 at four longitudinal locations in a hydraulic jump. The results illustrate the advective diffusion process with a broadening of the air-water shear region and the lesser maximum void fraction with increasing distance from the jump toe. Note that the void fraction is small at about middepth of the flow (Fig. 6). It is believed that this is

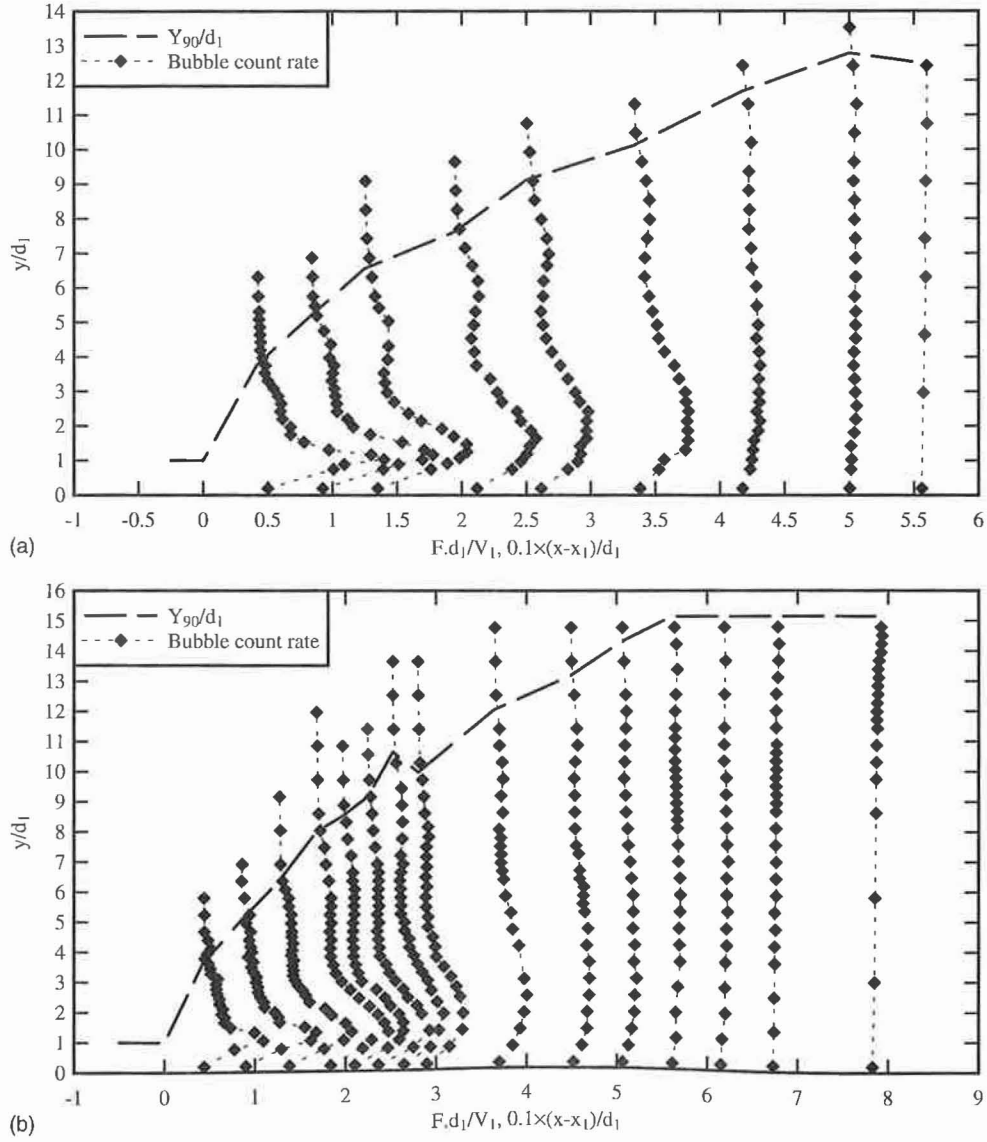

Fig. 7. Dimensionless distribution of bubble count rate $F \times d_1/V_1$—Horizontal axis: $0.1 \times (x - x_1)/d_1 + F \times d_1/V_1$; (a) $F_1 = 9.2$, $R = 6.9 \times 10^4$, $d_1 = 0.018$ m, $x_1 = 0.75$ m; (b) $F_1 = 11.2$, $R = 8.3 \times 10^4$, $d_1 = 0.01783$ m, $x_1 = 0.75$ m

related to the intense advective diffusion process at the largest Froude numbers; that is, the air bubbles are advected downstream very rapidly and do not have time to migrate to the upper flow region. This advective diffusion process yields a low void-fraction layer between the air-water shear layer and the upper free-surface region, as shown in Fig. 6.

Fig. 7 presents some dimensionless distributions of the bubble count rate $F \times d_1/V_1$ along the hydraulic jump for the same flow conditions shown in Fig. 5. The characteristic location Y_{90}/d_1 is shown also. For any bubble shape and size distribution, the bubble count rate is proportional to the air-water interface area and inversely proportional to the average bubble size for a given void fraction. It is simply proportional to the local rate of reaeration. In the hydraulic jump roller, the vertical profiles of the bubble count rate present a distinct, maximum count rate in the air-water shear layer; that is, $y/d_1 \sim 1$–2 in Fig. 7, depending on the longitudinal location. The local maximum bubble count rate in the shear layer is believed to be linked with the region of maximum shear stress. Above, the bubble count rate decreases with increasing distance from the invert, and it is equal to zero for $C = 1$ and for $C = 0$.

Some two-phase velocity measurements were conducted in the bubbly flow region with the dual-tip probe by using the mean interfacial travel time between the probe sensors (i.e., $\Delta x =$ 6.96 mm). Some typical results are presented in Fig. 8 for two Froude numbers (i.e., $F_1 = 7.5$ and 10.0). The figures present the dimensionless vertical distributions of interfacial velocities V/V_1 in the hydraulic jump roller. The dimensionless location of the measurement section is given in the legend. At the channel bed, a no-slip condition imposed $V(y = 0) = 0$. All the velocity profiles exhibited a similar shape despite some scatter. They followed the wall jet equations (Rajaratnam 1965; Gupta 1966; Chanson and Brattberg 2000). In the recirculation region above

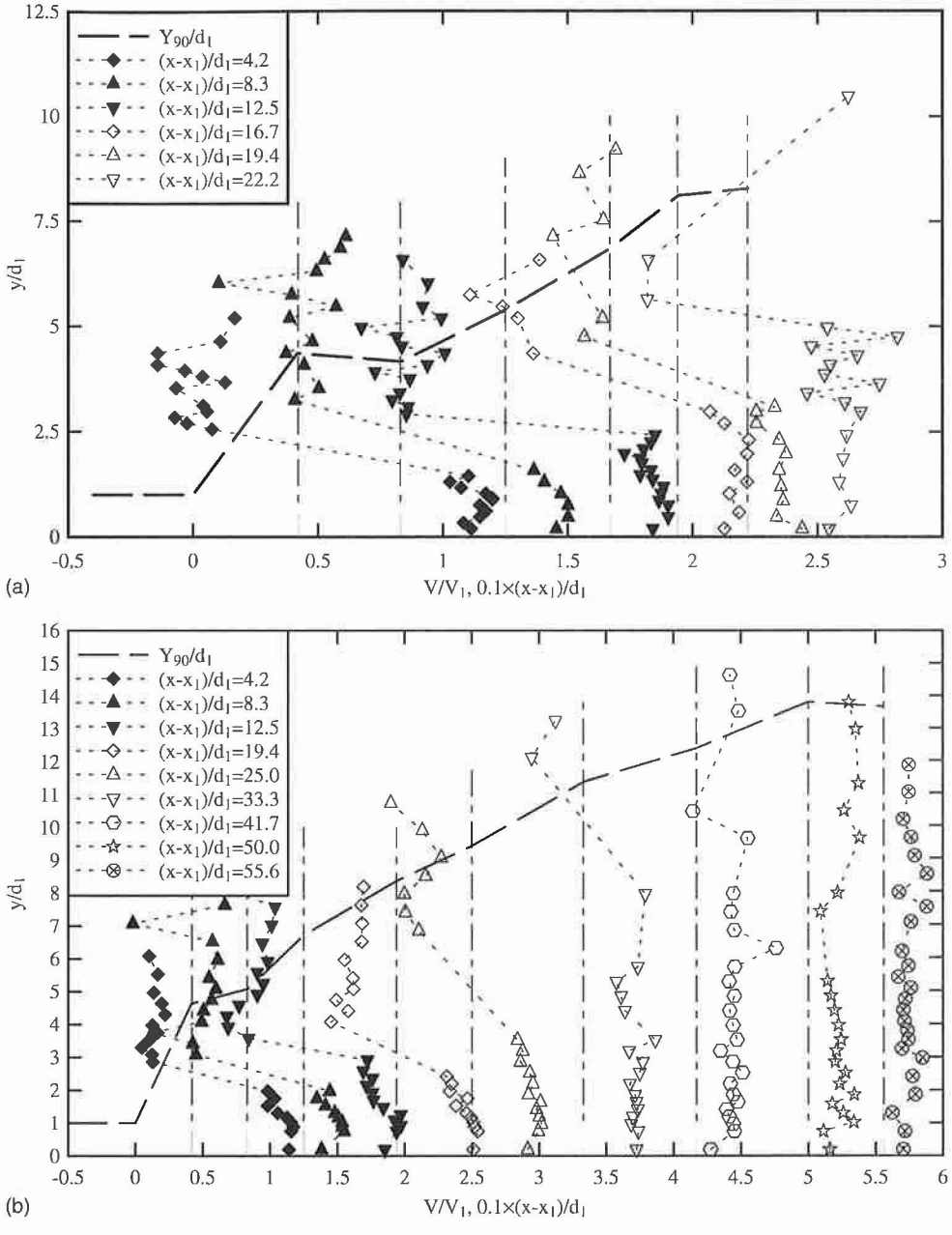

Fig. 8. Dimensionless velocity distributions V/V_1 in hydraulic jumps—Horizontal axis: $0.1 \times (x - x_1)/d_1 + V/V_1$; (a) $F_1 = 7.5$, $R = 5.6 \times 10^4$, $d_1 = 0.018$ m, $x_1 = 0.75$ m; (b) $F_1 = 10.0$, $R = 7.5 \times 10^4$, $d_1 = 0.018$ m, $x_1 = 0.75$ m

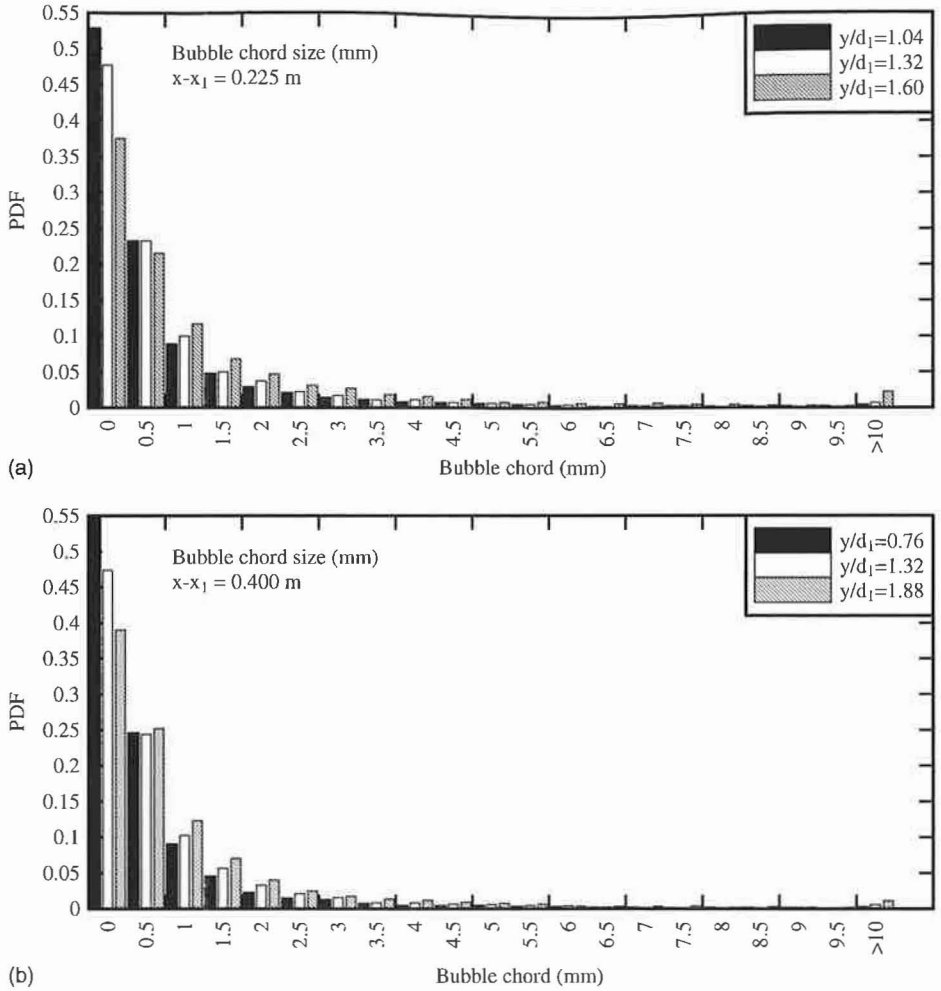

Fig. 9. Probability distribution functions of bubble chords in the shear layer: $F_1 = 11.2$, $R = 8.3 \times 10^4$, $d_1 = 0.01783$ m, $x_1 = 0.75$ m—Flow characteristics summarized in Table 2; (a) $x - x_1 = 0.225$ m; (b) $x - x_1 = 0.400$ m

the shear layer, the present data indicated some negative time-averaged velocities (Fig. 8). Whereas the probe design was not intended for some negative velocity measurements, the results showed that the recirculation motion was qualitatively observed with the dual-tip probe.

The bubble chord size measurements showed a broad spectrum of bubble sizes at each location. The range of bubble sizes extended over several orders of magnitude from less than 0.5 mm to more than 20 mm. Their distributions were skewed with a preponderance of small bubbles relative to the mean. In Fig. 9 corresponding to the air-water shear region, the probability of bubble size is the largest for chord times between 0 and 0.5 mm, although the mean size was between 2 and 6 mm. The probability distribution functions of bubble size typically followed a log-normal distribution; a similar finding was observed by Resch et al. (1974) and Chanson (2007). Fig. 9 shows some typical normalized bubble chord size distributions in the developing shear layer. For each figure part, the caption provides the location $(x - x_1, y/d_1)$, the local air-water flow properties (C, F, V), and the average bubble size. The histogram columns represent the probability of the droplet chord time in a 0.5 mm chord interval. For example, the probability of a bubble chord from 1 to 1.5 mm is represented by the column labeled 1 mm. Bubble sizes larger than 10 mm are regrouped in the last column (i.e., > 10 mm).

Discussion

In the design of hydraulic structures and stilling basins, a relevant design parameter is the depth-averaged void fraction and the rate of air entrainment. In some cases, the flow aeration must be maximized; for example, for reoxygenation purposes. In other situations, flow aeration must be prevented or reduced; for example, to counteract the effect of flow bulking on sidewall heights. In each case, the amount of air entrainment and the air-water flow properties must be accurately predicted to optimize the system performances and to insure a safe operation.

Fig. 10 presents the longitudinal distributions of the depth-averaged void fraction C_{mean} in the hydraulic jump. C_{mean} is defined by Eq. (2) and characterizes the amount of entrained air because $C_{mean} = Q_{air}/(Q + Q_{air})$ where Q is the water discharge; and Q_{air} is the rate of air entrainment. The data consistently show a large rate of air entrainment in the jump, as well as a rapid deaeration of the flow with increasing distance from the jump toe [Fig. 10(a)]. For the data set, the longitudinal decay in depth-averaged void fraction is best correlated by

$$C_{mean} = 0.3387 \times F_1^{0.202} * \exp \left[(-0.103 + 0.0073 \times F_1) \times \frac{x - x_1}{d_1} \right] \quad (7)$$

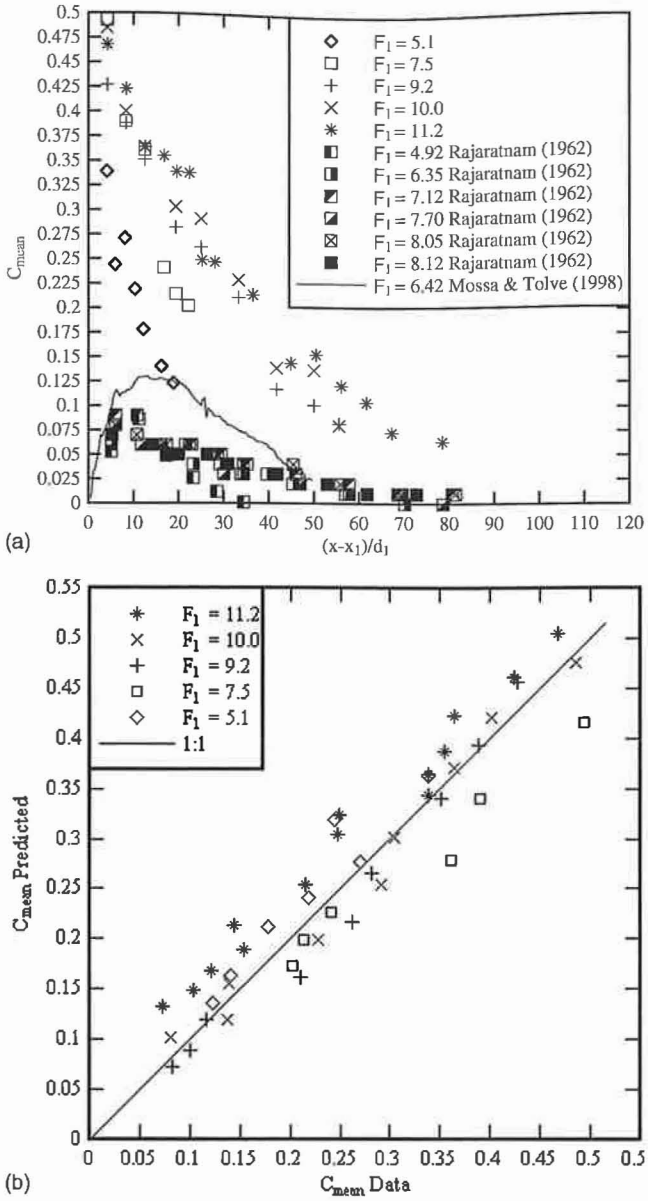

Fig. 10. Dimensionless longitudinal distributions of depth-averaged void fraction C_{mean} in hydraulic jumps; (a) comparison between the present data and previous studies (Rajaratnam 1962; Mossa and Tolve 1998); (b) comparison between the experimental data and Eq. (7)

Eq. (7) was compared with the data in Fig. 10(b). The agreement is reasonable with a normalized correlation coefficient of 0.947. The results imply a depth-averaged void fraction proportional to $F_1^{1/5}$, as well as a lower deaeration rate with increasing Froude numbers. That is, the rate of detrainment is comparatively small at the larger Froude numbers [Fig. 10(a) and Eq. (5)].

For comparison, the experimental data of Rajaratnam (1962) and Mossa and Tolve (1998) are shown in Fig. 10(a) and are compared with the present data. Note that Rajaratnam (1962) and Mossa and Tolve (1998) calculated their mean void fraction as an arithmetic mean rather than by using Eq. (2). The arithmetic mean is not a true depth-averaged void fraction [Eq. (2)].

Conclusion

Some detailed two-phase flow measurements were conducted in steady and strong hydraulic jumps with partially developed inflow. The measurements of jump toe fluctuations approximated earlier studies. The void-fraction distributions presented a local maximum in the air-water shear layer in which the distributions of void fractions were modeled by an advective diffusion equation. The shear zone was also characterized by a maximum in bubble count rate. The experimental observations highlighted a strong air entrainment rate. The depth-averaged void-fraction data demonstrated a large amount of entrained air, as well as a rapid deaeration of the jump roller, although the deaeration was comparatively small at the largest Froude numbers.

The results suggest that hydraulic jumps are effective aerators and that the dimensionless air content is retained longer at the largest Froude numbers; and thus, these jumps are better suited for use as an aeration device.

Acknowledgments

The writer thanks Ben Hopkins and Hugh Cassidy from the University of Queensland who carefully conducted the experimental measurements. He further acknowledges the financial support of the Australian Research Council with Grant No. DP0878922.

Notation

The following symbols are used in this paper:

C = void fraction defined as the volume of air per unit volume of air and water;
C_{max} = local maximum in void fraction in the developing shear layer;
C_{mean} = depth averaged void fraction $C_{mean} = \int_0^{Y_{90}} C \times dy$;
D_t = air bubble diffusivity (m^2/s) in the air-water shear layer;
$D^{\#}$ = dimensionless air bubble diffusivity $D^{\#} = D_t/(V_1 \times d_1)$;
d_1 = flow depth (m) measured immediately upstream of the hydraulic jump;
F = bubble count rate (Hz) defined as the number of bubbles that impact the probe sensor per second;
F_{max} = maximum bubble count rate (Hz) in the air-water shear layer;
F_{toe} = hydraulic jump toe oscillation frequency (Hz);
F_1 = upstream Froude number $F_1 = V_1/\sqrt{g \times d_1}$;
g = gravity acceleration (m/s^2) $g = 9.80$ m/s^2 in Brisbane, Australia;
h = sluice gate opening (m);
K = dimensionless constant;
L_{air} = hydraulic jump bubbly flow region length (m);
Q = water discharge (m^3/s);
Q_{air} = air flow rate (m^3/s);
R = Reynolds number $R = \rho \times V_1 \times d_1/\mu$;
T = average air-water interfacial travel time (s) between the two probe sensors;
V = air-water velocity (m/s);
V_1 = upstream flow velocity (m/s) $V_1 = Q/(W \times d_1)$;
W = channel width (m);
x = longitudinal distance from the upstream sluice gate (m);
x_1 = longitudinal distance from the upstream gate to the jump toe (m);
Y_{Cmax} = vertical elevation (m) at which the void fraction in the shear layer is maximum ($C = C_{max}$);
Y_{Fmax} = distance (m) from the bed at which the bubble count rate is maximum ($F = F_{max}$);
Y_{90} = characteristic distance (m) from the bed at which $C = 0.90$;

y = distance (m) measured normal to the flow direction;
Δx = longitudinal distance (m) between probe sensors;
δ = boundary layer thickness (m);
μ = dynamic viscosity (Pa · s) of water; and
ρ = density (kg/m^3) of water.

References

Babb, A. F., and Aus, H. C. (1981). "Measurements of air in flowing water." *J. Hydraul. Div.*, 107(HY12), 1615–1630.

Chanson, H. (1995). "Air entrainment in two-dimensional turbulent shear flows with partially developed inflow conditions." *Int. J. Multiphase Flow*, 21(6), 1107–1121.

Chanson, H. (1997). *Air bubble entrainment in free-surface turbulent shear flows*, Academic Press, London, 401.

Chanson, H. (2002). "Air-water flow measurements with intrusive phase-detection probes: Can we improve their interpretation?" *J. Hydraul. Eng.*, 128(3), 252–255.

Chanson, H. (2007). "Bubbly flow structure in hydraulic jump." *Eur. J. Mech. B, Fluids*, 26(3), 367–384.

Chanson, H. (2009a). "Advective diffusion of air bubbles in hydraulic jumps with large Froude numbers: An experimental study." *Hydraulic Model Rep. No. CH75/09*, School of Civil Engineering, Univ. of Queensland, Brisbane, Australia.

Chanson, H. (2009b). "Turbulent air-water flows in hydraulic structures: Dynamic similarity and scale effects." *Environ. Fluid Mech.*, 9(2), 125–142.

Chanson, H., and Brattberg, T. (2000). "Experimental study of the air-water shear flow in a hydraulic jump." *Int. J. Multiphase Flow*, 26(4), 583–607.

Chanson, H., and Gualtieri, C. (2008). "Similitude and scale effects of air entrainment in hydraulic jumps." *J. Hydraul. Res.*, 46(1), 35–44.

Crowe, C., Sommerfield, M., and Tsuji, Y. (1998). *Multiphase flows with droplets and particles*, CRC, Boca Raton, FL, 471.

Ervine, D. A., and Falvey, H. T. (1987). "Behaviour of turbulent water jets in the atmosphere and in plunge pools." *Inst. Civ. Eng. Proc.*, 83(1), 295–314.

Gupta, N. K. (1966). "Discussion of 'The hydraulic jump as a wall jet' by N. Rajaratnam." *J. Hydraul. Div.*, 92(HY3), 110–123.

Hager, W. H., Bremen, R., and Kawagoshi, N. (1990). "Classical hydraulic jump: Length of roller." *J. Hydraul. Res.*, 28(5), 591–608.

Henderson, F. M. (1966). *Open channel flow*, MacMillan, New York.

Kucukali, S., and Chanson, H. (2008). "Turbulence measurements in hydraulic jumps with partially-developed inflow conditions." *Exp. Therm. Fluid. Sci.*, 33(1), 41–53.

Liu, M., Rajaratnam, N., and Zhu, D. Z. (2004). "Turbulent structure of hydraulic jumps of low Froude numbers." *J. Hydraul. Eng.*, 130(6), 511–520.

Long, D., Rajaratnam, N., Steffler, P. M., and Smy, P. R. (1991). "Structure of flow in hydraulic jumps." *J. Hydraul. Res.*, 29(2), 207–218.

Mossa, M., and Tolve, U. (1998). "Flow visualization in bubbly two-phase hydraulic jump." *J. Fluids Eng.*, 120(1), 160–165.

Murzyn, F., and Chanson, H. (2008). "Experimental assessment of scale effects affecting two-phase flow properties in hydraulic jumps." *Exp. Fluids*, 45(3), 513–521.

Murzyn, F., and Chanson, H. (2009). "Free-surface fluctuations in hydraulic jumps: Experimental observations." *Exp. Therm. Fluid. Sci.*, 33(7), 1055–1064.

Murzyn, F., Mouaze, D., and Chaplin, J. R. (2005). "Optical fibre probe measurements of bubbly flow in hydraulic jumps." *Int. J. Multiphase Flow*, 31(1), 141–154.

Murzyn, F., Mouaze, D., and Chaplin, J. R. (2007). "Air-water interface dynamic and free surface features in hydraulic jumps." *J. Hydraul. Res.*, 45(5), 679–685.

Rajaratnam, N. (1962). "An experimental study of air entrainment characteristics of the hydraulic jump." *J. Inst. Eng. (India)*, 42(7), 247–273.

Rajaratnam, N. (1965). "The hydraulic jump as a wall jet." *J. Hydraul. Div.*, 91(HY5), 107–132.

Rao, N. S. L., and Kobus, H. E. (1971). "Characteristics of self-aerated free-surface flows." *Water and waste water: Current research and practice*, Vol. 10, Eric Schmidt Verlag, Berlin.

Resch, F. J., Leutheusser, H. J., and Alemu, S. (1974). "Bubbly two-phase flow in hydraulic jump." *J. Hydraul. Div.*, 100(HY1), 137–149.

Rouse, H., Siao, T. T., and Nagaratnam, S. (1959). "Turbulence characteristics of the hydraulic jump." *Trans. Am. Soc. Civ. Eng.*, 124, 926–950.

Wood, I. R. (1991). "Air entrainment in free-surface flows." *IAHR Hydraulic Structures Design Manual No. 4: Hydraulic Design Considerations*, Balkema, Rotterdam, The Netherlands, 149.